CONF-800455--2

ENERGY AND ANGULAR DISTRIBUTION OF LOW ENERGY H^+ AND D^+ BACKSCATTERED FROM POLYCRYSTALLINE CARBON*

S. H. Overbury, P. F. Dittner, S. Datz

Oak Ridge National Laboratory
Oak Ridge, Tennessee 37830

and

R. S. Thoe

Oak Ridge National Laboratory

and

The University of Tennessee
Knoxville, Tennessee 37916

*Research sponsored by the Division of Chemical Sciences, Office of Basic Energy Sciences, U. S. Department of Energy, under contract W-7405-eng-26 with the Union Carbide Corporation.

DISCLAIMER

Abstract

The energy distributions of H^+ and D^+ backscattered from a polycrystalline graphite sample were recorded as a function of total scattering angle, angle of incidence, and for incident beam energies $200 < E_i < 3000$ eV. The general shapes of the distributions are discussed qualitatively, and their variation with incident energy and total scattering angle are explained and compared with theoretical and other experimental results. The average energies $\bar{E}^+$ of the distributions are found to increase relative to the single scattering energy, E_k, with decreasing incident energy. $\bar{E}^+/E_k$ also increases with decreasing exit angle from the solid in a way which is slightly dependent upon the angle of incidence. The integrated intensities of the distributions are found to depend strongly upon the angle of incidence, with a normally incident beam producing a nearly cosine distribution of backscattered ions and grazing angles of incidence producing an intensity which peaks at an angle forward of the specular direction. Using charge fractions obtained previously for surface scattering from graphite and transmission through thin carbon foil, values of the particle reflection coefficient R_N are obtained as a function of energy.

Introduction

The interaction of low energy ($\lesssim$ 3000 eV) protons or hydrogen atoms with solids is of interest in the understanding of the effects of TOKOMAK plasmas on "first wall" materials. A comprehensive physical picture of the interaction requires a knowledge of the stopping power, energy and particle "reflection", single and multiple scattering behavior, and the charge fractions of reflected particles.

Complementing our previous work on stopping power, emergent charge state fractions, and angular distributions of hydrogen and deuterium transmitted through thin carbon foils [1] and upon charged fractions of elastically backscattered H [2] we report here on the energy and angular distributions of hydrogen reflected from carbon.

Experimental

Apparatus. The basic apparatus is only slightly modified from that described earlier [1]. The vacuum system consisted of a scattering chamber ($P = 5 \times 10^{-7}$ Pa) pumped by a turbo-molecular pump and a liquid nitrogen cooled Ti sublimator and a separately pumped source chamber ($P = 1 \times 10^{-5}$ Pa). The ions were extracted from a Colutron discharge ion source, focused, and mass analyzed by a Wien filter. Two beam defining apertures (which also provided differential pumping) limited the beam flux to a maximum divergence of $\pm 1^{\circ}$ and gave a beam spot diameter of about 2 mm at the sample.

The backscattered ion spectra were measured with a rotatable spherical electrostatic analyzer (ESA) having 3% energy resolution, and a field free region between the sample and the analyzer entrance apertures (2.5 mm dia.).

The geometric solid angle defined by the entrance apertures of the analyzer and their distance from the sample was 4 msr. The ESA could be set for total scattering angles, θ, of 0 to 130° from the initial beam direction. The angle of incidence, ψ, between the beam direction and the surface plane could be varied and the axis of rotation of the sample was set to be identical to the axis of rotation of the ESA and was located in the surface of the sample.

The beam current collected from the sample, I_c, was integrated to obtain a total fluence. This was then corrected for secondary electron emission which is a function of the incident energy, E_i and ψ and was measured after each spectrum. The correction to I_c for reflected ions is negligible.

Backscattering Measurements. Energy spectra of the backscattered positive ions were collected as a function of θ,ψ and E_i for incident H^+, H_2^+, D^+ or D_2^+. The raw spectrum were smoothed and corrected for the 1/E distortion of the ESA, and using the secondary electron emission correction and the collected beam current, they were scaled to a fixed beam fluence of 1.0 μC. No correction was made for the analyzer transmission which was unknown or the efficiency of the channeltron which we believed to be near unity at the accelerating potentials used. The resultant spectra are then distributions of the reflected positive ions $N^+(E)$ as a function of the final energy after reflection, E. The average energy $\bar{E}^+$ and the total integrated intensities N_T^+ for each distribution can be obtained straightforwardly.

The sample used was a fine-grained polycrystalline graphite strip (6 x 30 x 0.9 mm) with a density of 1.90 gm/cm^3 which was polished to a mirror finish, de-dusted in liquid nitrogen and rinsed in ethanol. In vacuum, the sample was heated frequently to about 950°C to drive off surface impurities and implanted hydrogen. The surface purity could only be estimated from the backscattering spectra. A small increase in the backscattered intensity near

the single scattering energy for H^+ from oxygen and occasionally an even smaller increase corresponding to a mass near Na could be observed at the largest scattering angles. He^+ backscattering spectra which might indicate impurities were difficult to obtain due to low signal levels (caused presumably by very high neutralization probability) but gave small peaks at energies expected for C and O. Ar^+ backscattering spectra gave only a large secondary ion tail with no structure indicative of high Z impurities.

There were certain non-reproducibilities in the shape and intensity of the spectra that were observed when different points across the sample were compared. $\bar{E}^+$ was found to vary by 3-5% while N_T was subject to variations of up to 20%. For consistency, the measurements reported below were obtained from a single point on the sample. An attempt was made to produce such a variation at a single point by exposing the sample to H_2^+ irradiation ($\sim$ 100 μC of H_2^+ at 500 eV/amu) and comparing the H^+ backscattered spectrum with the corresponding distribution obtained after heating the sample in accordance with the usual procedure. The H_2^+ irradiation appeared to cause a very slight decrease in $\bar{E}^+$ ($\sim$ 1%) and an increase (8-9%) in N_T^+. Such an irradiation was far in excess of that required to collect a series of spectra (0.5 to 2 μC per spectrum). No long term effects could be discerned in a comparison of earlier and later results indicating that repeated heating and exposure to H^+ irradiation did little to affect the backscattered distributions. The repeatability of the values of N_T^+ and $\bar{E}^+$ are of the order of ±5% and ±1% respectively and indicate the cumulative random experimental error due to such sources as the uncertainties in the secondary electron emission correction and in the positioning of θ and ψ.

Results

Typical H^+ and D^+ backscattering spectra are shown in Fig. 1 for a fixed scattering angle $\theta = 90°$ but with different E_i. The lowest energy H^+ spectrum (E_i = 100 eV) was obtained using a beam of H_2^+ at an accelerating potential of 200 V, but the other $H^+(D^+)$ spectra were recorded using $H^+(D^+)$ at the indicated energy. When compared at the same incident energy per amu, H^+ and H_2^+ give qualitatively the same shape spectra, as do D^+ and D_2^+. A rather pronounced cutoff or "kinematical edge" on the high energy side of each spectrum was observed near the energy $E_k = 0.846\ E_i$ ($= 0.714\ E_i$) appropriate for elastic scattering of an $H^+(D^+)$ ion from a C atom at $\theta = 90°$. The width of this edge for the highest energies is determined principally by the energy resolution of the ESA, but there appears to be additional broadening of the edge for the lowest values of E_i especially for D^+. Below the kinematical edge, the distributions show a broad maximum that is most pronounced for the highest incident energies and below which the intensity drops off to zero with decreasing energy. The spectra in Fig. 1 demonstrate that the broad maximum in the distribution shifts closer to the kinematical edge with decreasing energy. To demonstrate the effect more clearly, the average energy $\bar{E}^+$ divided by E_i (both in eV/amu) is shown as a function of E_i in Fig. 2 for incident H^+, H_2^+, D^+ and D_2^+.

A shift in the distributions towards the kinematical edge is observed for decreasing exit angle. This is demonstrated by the energy distribution in Fig. 3 and in Fig. 4 where the average energy of each distribution divided by the kinematical single scattering energy appropriate for the incident energy and total scattering angle is plotted versus the exit angle measured from the plane of the surface (θ-ψ). The data are shown for different angles of incidence

and for a wide range of total scattering angles. A general increase in $\bar{E}^+/E_k$ is observed with decreasing exit angle. There also appears to be a slight dependence upon angle of incidence which is more pronounced at E_i = 1000 eV than at 2000 eV.

In Fig. 5 the integrated intensities of the distributions are given as a function of θ and ψ for two different incident energies. For normal incidence the integrated intensity follows a cosine distribution rather closely and a least square fit to the data for such a distribution is given. At grazing angles of incidence the intensity always peaks slightly forward of the specular angle (indicated by the arrows) with the sharpest peaking occuring for the most grazing angles.

Discussion

The fact that incident H^+ and H_2^+ at twice the accelerating potential give H^+ backscattering spectra which have identical shapes is in agreement with the expectation that H_2^+ quickly dissociates into two protons (or atoms) each carrying half the incident energy. For H_2^+ incident energy E_i = 100 and 200 eV/amu, no H_2^+ ions backscattered through 90° were observed down to a sensitivity of $\sim$ 0.5% of the backscattered H^+ signal. H_2^+, D_2^+ and D_3^+ have been observed to survive backscattering from metals [3,4], although the fraction of H or D surviving in molecules is low and decreases sharply with increasing energy transfer of the collision. The present failure to observe H_2^+ under these scattering conditions (E_i > 100 eV, θ = 90°) is consistent with those results.

It is interesting to note that for H^+ and D^+ incident with the same velocity, the resulting H^+ and D^+ backscattering spectra are seen to have a similar shape if they are compared at the same exit velocity or energy per amu.

Such a comparison is shown in Fig. 6. The low energy portions of the spectra are identical in shape up to near the cut-off in the D^+ spectrum at the kinematical single scattering E_k, which is lower for D^+ than for H^+. This explains the lowering of $\bar{E}^+/E_i$ for the D^+ spectrum below that for H^+ at any given incident energy per amu (Fig. 2). As E_i increases, the portion of the spectrum near E_k becomes less important relative to the lower energy portion, so $\bar{E}^+/E_i$ for D^+ should come closer to that for H^+.

The steady increase of $\bar{E}^+/E_i$ with decreasing E_i is in agreement with results of Eckstein and Verbeck [5] for various materials at higher E_i and can be qualitatively understood by comparison with other results at other energies [6,7]. At the higher energies used in Rutherford backscattering experiments, the distribution of particles backscattered from smooth solid surfaces show a monotonic increase in intensity with decreasing emergent energy which is caused by the single scattering nature of the spectrum and the increase of the scattering cross section with decreasing energy [6]. At sufficiently lower energies, depending upon the ion-target combination, backscattering spectra exhibit peaks near E_k in both the ion and neutral particle spectra that can be attributed to very large scattering cross sections which prevent significant penetration and inelastic energy loss for most incident particles [7]. The results presented here represent an energy range between these extremes and the transition between ranges is manifested in the shift of the broad maximum and of $\bar{E}^+$ towards E_i (or E_k) with decreasing E_i.

The shift towards higher energy with decreasing θ observed in the backscattered H^+ distribution (Fig. 3) is partly due to the lower momentum transfer required to scatter through a smaller scattering angle θ, and this causes the kinematical edge to move toward higher energy. But, the broad multiple scattering peak also moves towards higher energies as indicated by the increase

in $\bar{E}^+/E_k$ with decreasing θ (Fig. 4). This shift occurs because the low energy portions of the spectra exhibit nearly a cosine angular distribution while the high energy regions are peaked near the specular angle.

It should be pointed out that the backscattering is very dependent upon the incidence angle ψ indicating that the backscattered particles do not lose complete "memory" of their initial direction. A comparison of energy distributions obtained for the same exit angle and E_i, but for different ψ, shows that the shapes are different and $\bar{E}^+/E_k$ increases systematically with decreasing ψ. This was found at E_i = 1000 and 2000 eV. To a lesser extent $\bar{E}^+/E_k$ also increases with decreasing ψ as seen in Fig. 4. The angular distributions of total intensity, N_T^+, shown in Fig. 5 are also dependent upon ψ. The peaking of the angular distribution near the specular angle for grazing angles of incidence has been experimentally observed previously [8] and a cosine distribution for normal incidence has been obtained from computer simulations [9]. Those calculations also predicted an increase in total reflection coefficient with decreasing ψ which would explain the corresponding increase of N_T^+ observed (Fig. 5).

Only the charged particle distributions $N^+(E)$ have been measured here. To obtain the total particle energy spectrum N(E) from $N^+(E)$ requires a knowledge of the energy dependent charge fraction $f^+(E)$. f^+ has been measured for H transmitted through thin carbon foils [1], for bulk backscattered H [10] and for surface backscattered H [2]. For H^+ ions exiting normal from a foil after passing through about 150-200 Å of amorphous carbon, the charge fraction was found to depend roughly linearly upon the final energy E [1]. Bhattacharya, et al. [10] determined that for normally incident H^+ backscattered through 135° from within graphite, f^+ increased monotonically with E dependence which is somewhat weaker than linear for E < 2keV. Their experiments differed from the

thin foil experiments in that the observed particles probably suffered at least one wide angle scattering event. Finally from the step height of the kinematical edge, f^+ for hydrogen single scattered from the surface of graphite was found to depend not only upon the final energy but upon the perpendicular components of the initial and final velocities, $v_{i\perp}$ and $v_{f\perp}$ [2]. A good empirical fit to the data was given by $f^+ = C_1 v_{f\perp} + C_2 v_{i\perp}$ where C_1 and C_2 are constants. This result applies only to elastically single scattered particles and, for fixed entrance and exit angles, this form reduces to $f^+ \sim E^{\frac{1}{2}}$ with a constant of proportionality which depends upon θ and ψ. All three of the above results agree that qualitatively $f^+ \sim AE^m$ with m varying between ½ and 1.

The resulting shapes of the total particle distribution N(E) obtained from $N^+(E)/f^+(E)$ will depend upon m, but not upon A as long as A is independent of E. Thus uncertainty in A will only appear as a uncertainty in the absolute intensity. It is found that N(E) obtained using this form of $f^+(E)$ maintains the basic features of $N^+(E)$, i.e., there is a kinematical edge, a broad maximum at lower energy and intensity which drops off toward zero below the maximum. There is, however, a shift of the maximum in intensity towards lower energy as might be expected for f^+ of this form. The shift is more severe for m = 1 than for m = ½. For m = 1, $\bar{E}$ is uniformly lower than $\bar{E}^+$ by about 10-12% of the kinematical energy for all incident energies for both H and D.

A total particle reflection coefficient, R_N, is also obtainable from these data, however, since no out-of-plane scattering data was obtained, it is not possible to get a total reflection yield for a non-normal beam incidence. For normal incidence on a polycrystalline target it is reasonable to assume that the backscattered intensity is azimuthally independent. The data in Fig. 5 indicate that N_T^+ varies perhaps only slightly more slowly than cosine

dependence. If the $N^+(E)$ is corrected for charge fraction ($f^+ = AE$) to obtain N(E) and then a total integrated intensity N_T is computed for this distribution, virtually the same dependence upon polar exit angle is again found, as long as A is independent of angle. The deviation from cosine dependence which is larger for the lower energies and larger for D^+ than for H^+ at the same E_i, causes uncertainty in extrapolating N_T^+ to normal exit angles as necessary for obtaining R_N. Assuming a value for A of 0.03/keV for H^+ [1] and using half of the value for D^+ as suggested by Bhattacharya [10], it is possible to compute N_T and then R_N. The results obtained with these assumptions are shown in Fig. 7 along with experimental results of Eckstein and Verbeek [5] and results of a simulation made using the computer code MARLOWE for H on an amorphous carbon foil which was infinitely thick with respect to reflection. The error bars in Fig. 7 reflect the uncertainties in R_N due to a random experimental error and estimated errors arising from the extrapolation of N_T. Figure 7 indicates a small systematic difference between H^+ and D^+ results which is not presently understood. The computed and experimental results for H^+ are all in good agreement.

Acknowledgements

We are deeply grateful to M. T. Robinson for many useful discussions and for graciously providing the computer results.

References

1. S. H. Overbury, P. F. Dittner, S. Datz and R. S. Thoe, Rad. Effects 41, (1979) 219.

2. S. H. Overbury, P. F. Dittner and S. Datz, Nucl. Instr. Meth., in press.

3. W. Heiland, U. Beitat and E. Taglauer, Phys. Rev. B 19 (1979) 1677.

4. W. Eckstein, H. Verbeek and S. Datz, Appl. Phys. Lett. 27 (1975) 527.

5. W. Eckstein and H. Verbeek, J. Nucl. Mat. 76 & 77 (1978) 365.

6. W. K. Chu, J. W. Meyer and M. A. Nicolet, Backscattering Spectrometry, (Academic Press, New York, 1978).

7. T. M. Buck, Y. S. Chen, G. H. Wheatley and W. F. Van der Weg, Surf. Sci. 47 (1975) 244.

8. W. Eckstein and H. Verbeek, J. Vac. Sci. Techn. 9 (1971) 612.

9. O. S. Oen and M. T. Robinson, Nucl. Inst. Meth. 132 (1976) 647.

10. R. S. Bhattacharya, W. Eckstein and H. Verbeek, Surf. Sci., in press.

11. J. Lindhard, M. Scharff and H. E. Schiøtt, Kgl. Danske Videnskab. Selskab, Mat.-Fys. Medd. 33, no. 14 (1963).

Figure Captions

Fig. 1. The energy distribution of backscattered a) H^+ and b) D^+ from carbon are shown. H_2^+ was used as the incident beam for the lowest energy H^+ spectrum (E_i = 100eV/amu) but other H^+ and D^+ spectra were generated using H^+ and D^+ respectively as the incident beam at the incident energies, indicated in eV.

Fig. 2. The average energy $\bar{E}^+$ in eV/amu for ν H^+ and D^+ backscattered distributions normalized to the incident energy E_i in eV/amu are plotted against E_i. Results are shown for four different incident projectiles.

Fig. 3. H^+ backscattering spectra are shown for various total scattering angles θ with 1000eV H^+ incident.

Fig. 4. The average energy $\bar{E}^+$, of backscattered H^+ normalized to the kinematical single scattering energy E_k is shown as a function of the exit angle $(\theta-\psi)$ for various incident energies E_i and incident angles ψ.

Fig. 5. The angular variation of the integrated intensity of the backscattered H^+ energy distribution is shown for various incident energies E_i and incident angles ψ. The curves are drawn visually to indicate the trends of the data.

Fig. 6. H^+ and D^+ energy distributions for incident 1000eV H_2^+ and 1000eV D^+ are plotted versus the energy of the scattered particle divided by its mass in amu.

Figure Captions (Cont'd.)

Fig. 7. The total particle reflection coefficient R_N is shown as a function of Lindhard's reduced energy ε [11]. To obtain the energy E_i of the normally incident H^+ or D^+, multiply ε by 413 eV or 445 eV respectively. Results calculated using the computer code MARLOWE and experimental results from [5] are shown for comparison. The curve is drawn visually to indicate the trend of the H^+ data.

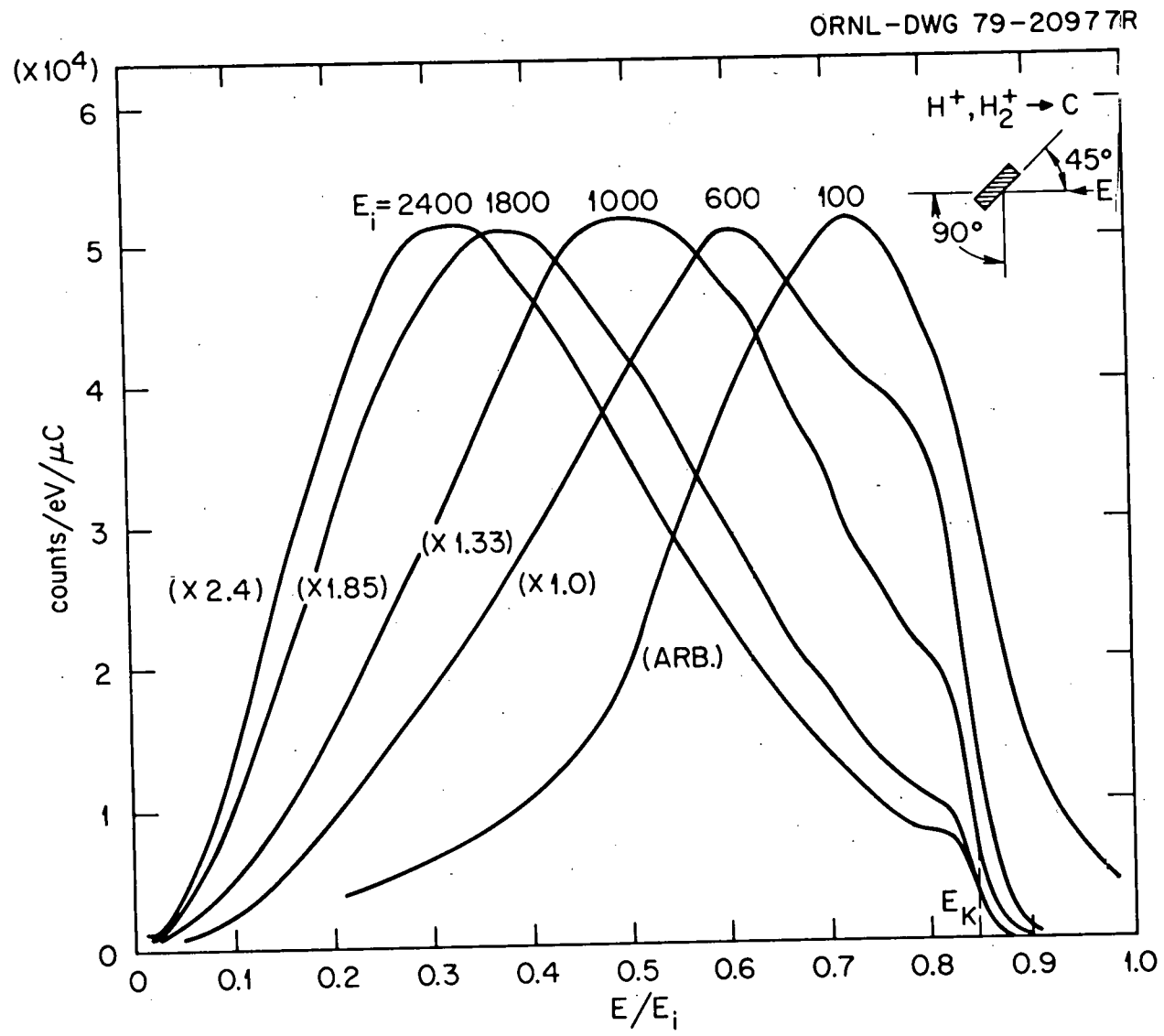
ORNL-DWG 79-20977R
(X10^4)
counts/eV/μC
E/E_i
E_i = 2400 1800 1000 600 100
(X 2.4)
(X1.85)
(X 1.33)
(X 1.0)
(ARB.)
E_K
H+, H2+ → C
45°
E_i
90°

Fig. 1a

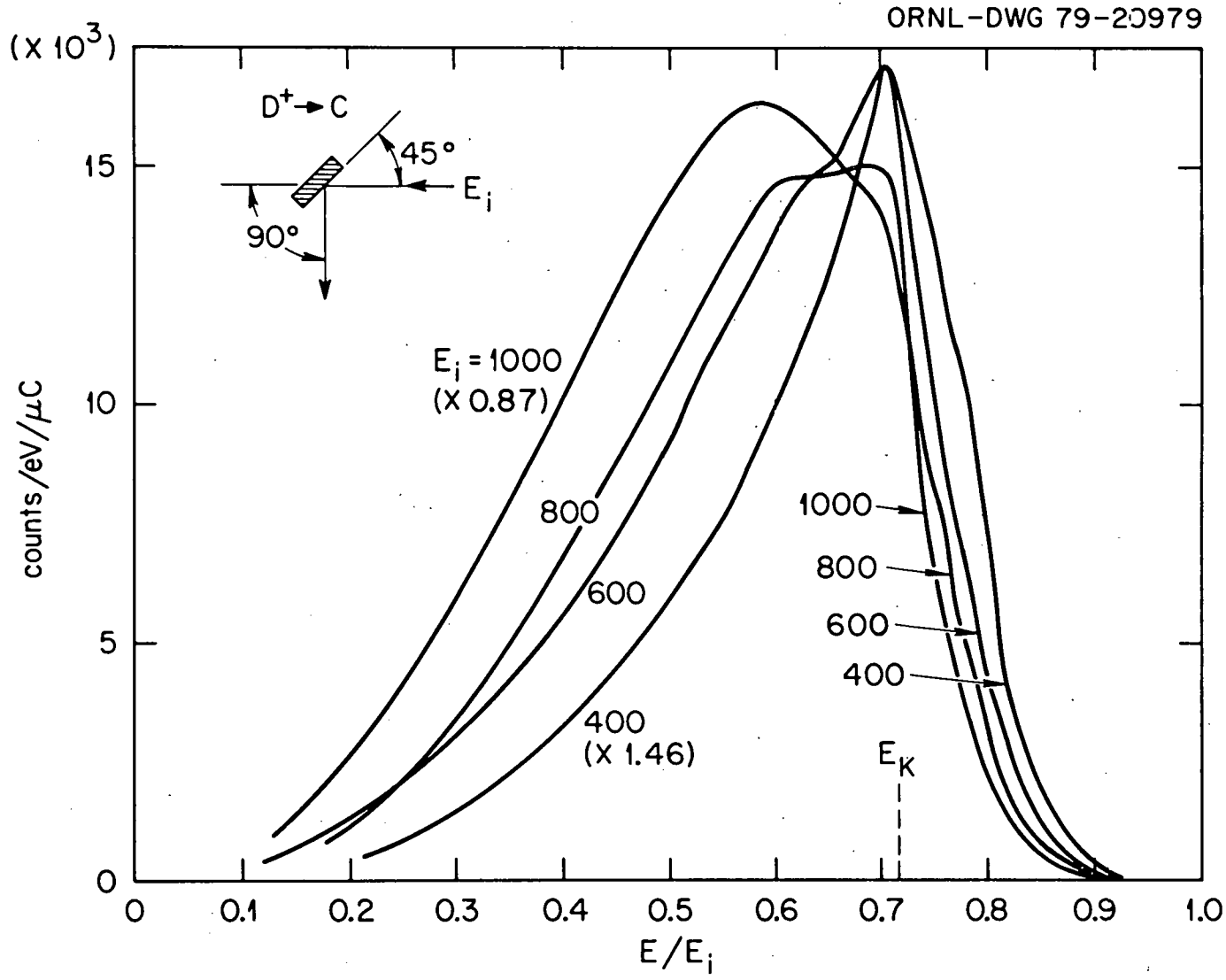
ORNL-DWG 79-20979
(X 10³)
counts/eV/μC
D⁺ → C
45°
E_i
90°
E_i = 1000
(X 0.87)
800
600
400
(X 1.46)
1000
800
600
400
E_K
0
5
10
15
0
0.1
0.2
0.3
0.4
0.5
0.6
0.7
0.8
0.9
1.0
E/E_i

Fig. 1b

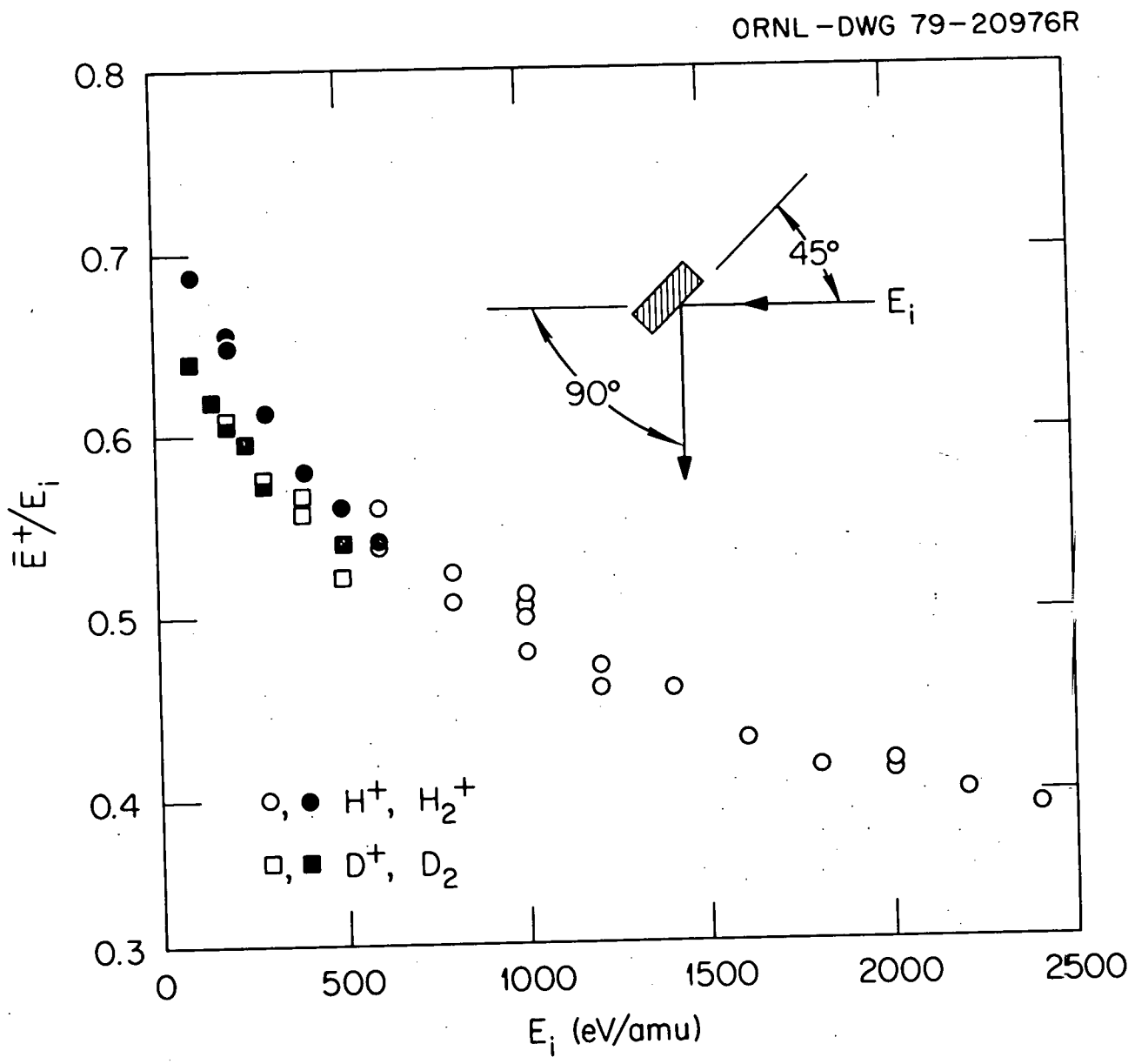
ORNL-DWG 79-20976R
0.8
0.7
0.6
0.5
0.4
0.3
0
500
1000
1500
2000
2500
E^+/E_i
E_i (eV/amu)
45°
E_i
90°
○, ● H^+, H_2^+
□, ■ D^+, D_2

Fig. 2

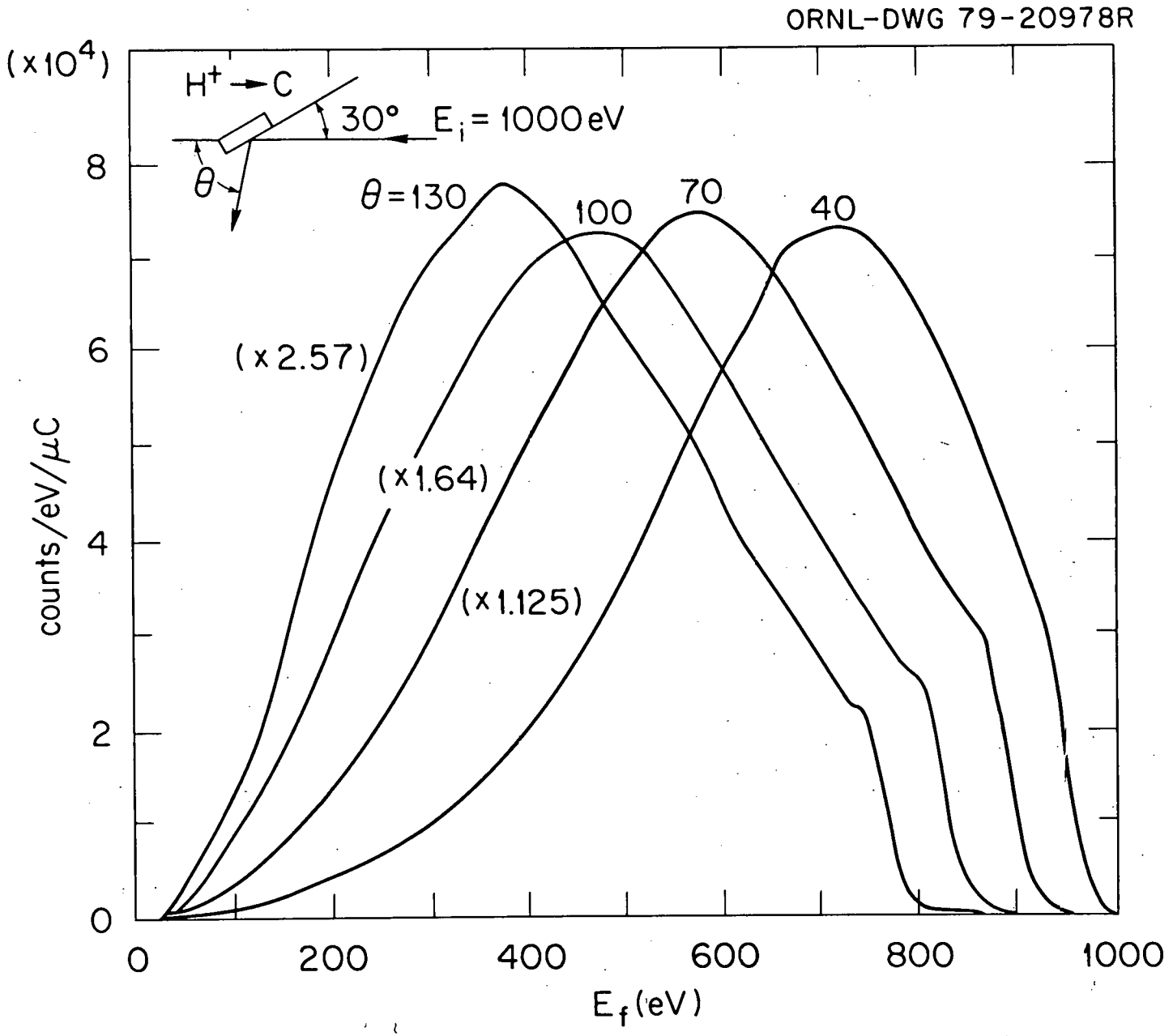
ORNL-DWG 79-20978R
(x10^4)
H+ → C
30°
E_i = 1000 eV
θ
θ=130
100
70
40
(x2.57)
(x1.64)
(x1.125)
counts/eV/μC
E_f (eV)
0
2
4
6
8
0
200
400
600
800
1000

Fig. 3

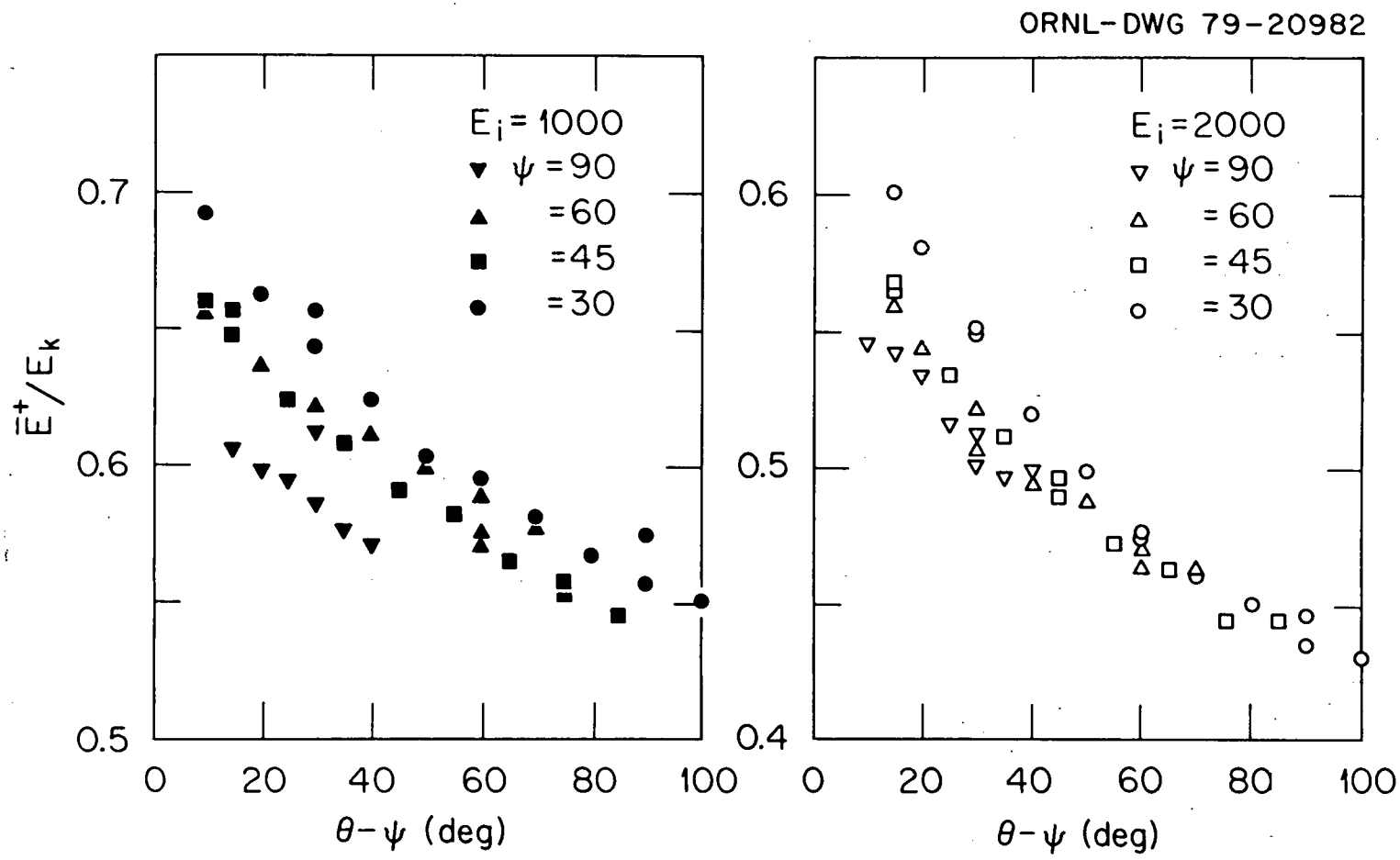
ORNL-DWG 79-20982
E_i = 1000
ψ = 90
= 60
= 45
= 30
E_i = 2000
ψ = 90
= 60
= 45
= 30
$\bar{E}^+/E_k$
0.7
0.6
0.5
0.6
0.5
0.4
0
20
40
60
80
100
θ−ψ (deg)

Fig. 4

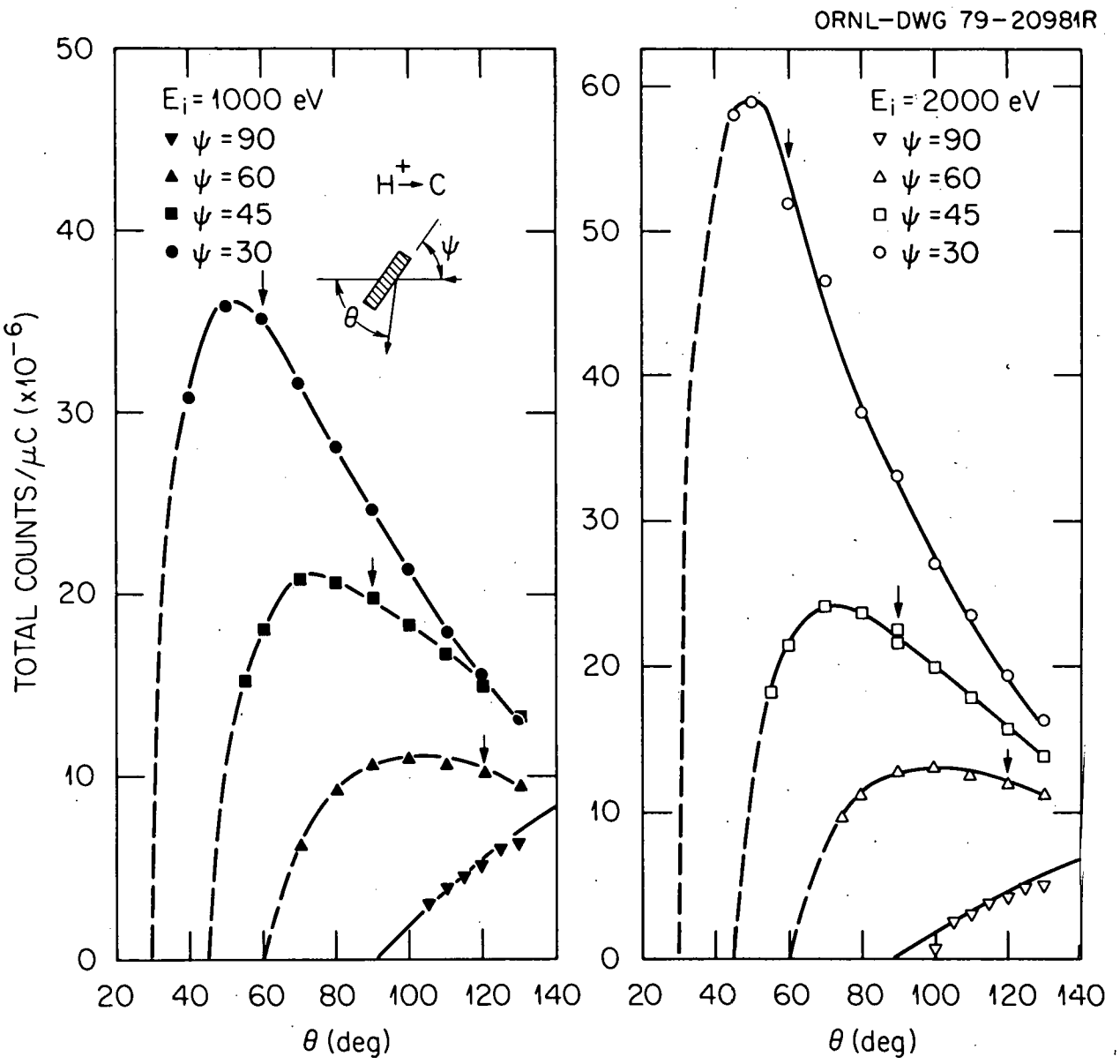
ORNL-DWG 79-20981R
E_i = 1000 eV
▼ ψ = 90
▲ ψ = 60
■ ψ = 45
● ψ = 30
$H^+ \rightarrow C$
ψ
θ
TOTAL COUNTS/μC (x10^{-6})
θ (deg)
E_i = 2000 eV
▽ ψ = 90
△ ψ = 60
□ ψ = 45
○ ψ = 30
θ (deg)

Fig. 5

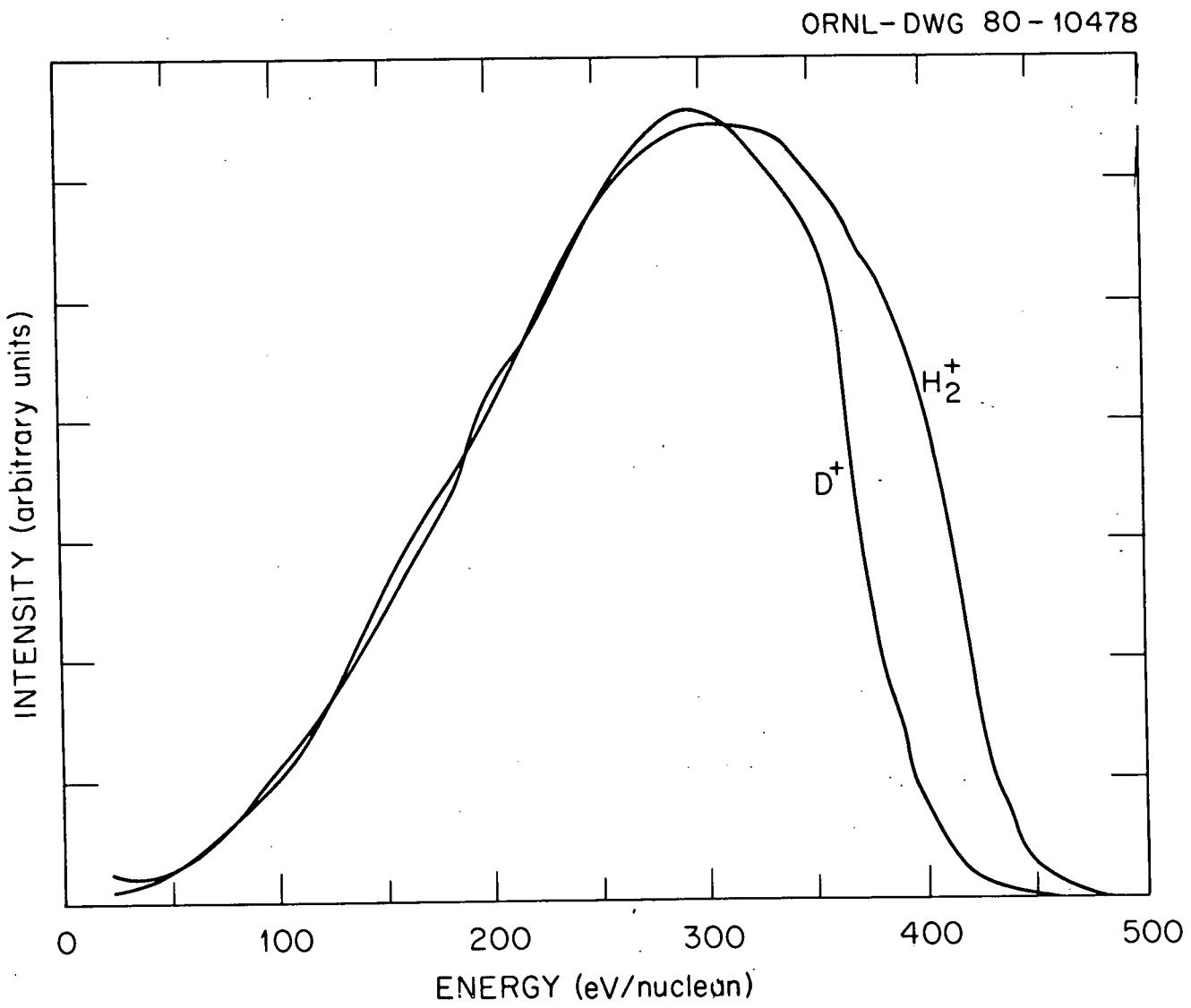
ORNL-DWG 80-10478
INTENSITY (arbitrary units)
H_2^+
D^+
0
100
200
300
400
500
ENERGY (eV/nucleon)

Fig. 6

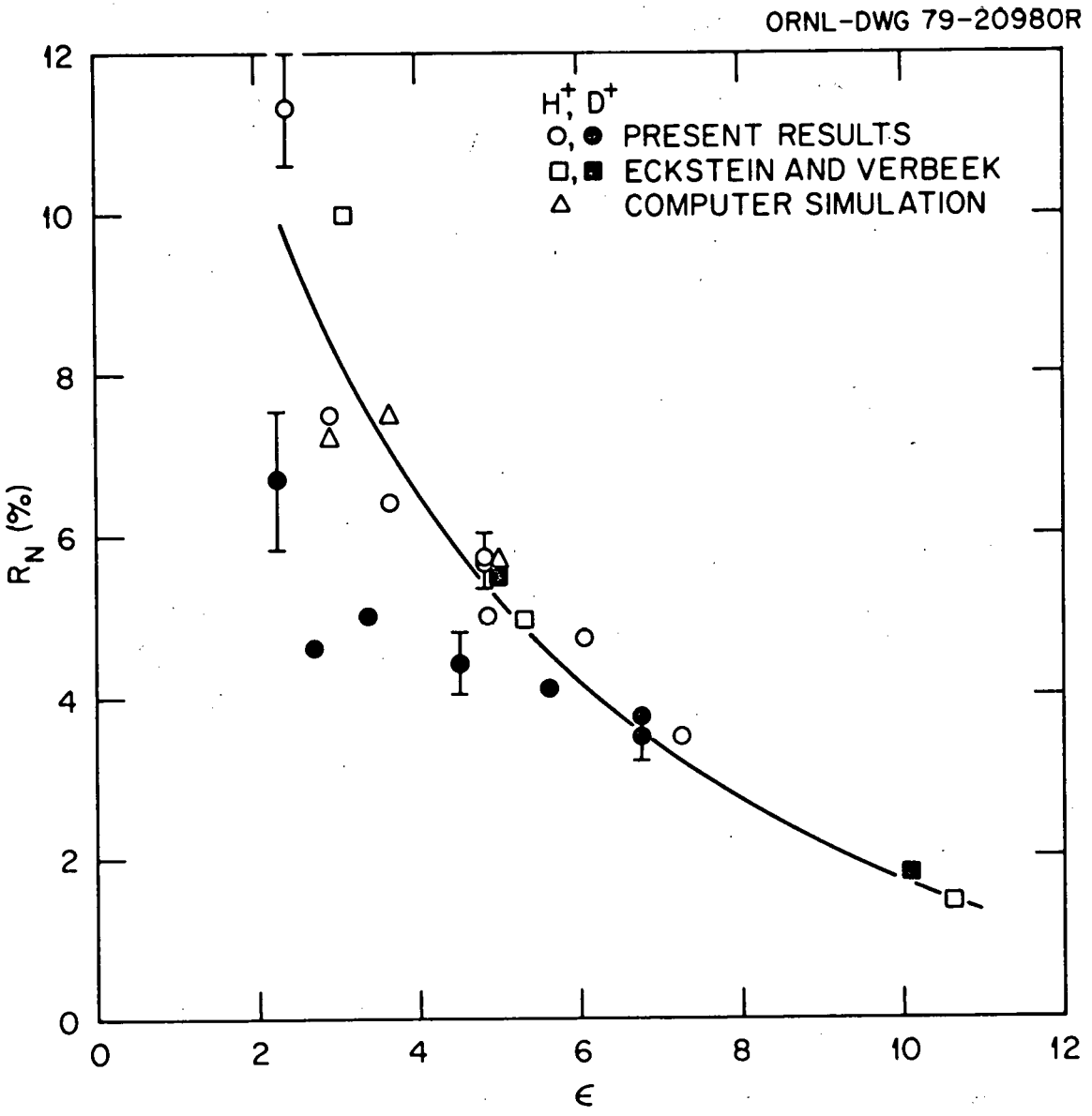
ORNL-DWG 79-20980R
H+, D+
PRESENT RESULTS
ECKSTEIN AND VERBEEK
COMPUTER SIMULATION
R_N (%)
ε
0
2
4
6
8
10
12

Fig. 7